Geoderma 154 (2010) 267–280

Contents lists available at ScienceDirect

Geoderma

journal homepage: www.elsevier.com/locate/geoderma

Interrelation of magnetic susceptibility, soil color and elemental mobility in the Pliocene–Pleistocene Siwalik paleosol sequences of the NW Himalaya, India

V. Kumaravel [a,b], S.J. Sangode [a,c,*], N. Siva Siddaiah [a], Rohtash Kumar [a]

[a] Wadia Institute of Himalayan Geology; 33, General Mahadeo Singh Road, Dehra Dun-248 001, India
[b] K.S. Krishnan Geomagnetic Research Laboratory (IIG), Leelapur Road; Chamanganj, Allahabad-221 505, India
[c] Department of Geology, University of Pune, Ganeshkhind, Pune-411 007, India

ARTICLE INFO

Article history:
Received 17 March 2009
Received in revised form 3 October 2009
Accepted 17 October 2009
Available online 13 November 2009

Keywords:
Magnetic susceptibility
Elemental mobility
Soil color
Paleosols
Siwaliks
Himalayan Foreland Basin

ABSTRACT

Apart from imparting color characteristics, the precipitation and dissolution of Fe-oxides (and hydroxides) during pedogenesis is coeval with transformation and translocation of major and trace elements. Based on rock magnetic and geochemical parameters for 27 paleosol profiles from three stratigraphic columns of Pliocene–Pleistocene Siwalik sequence in the NW Himalaya, we describe here the relationship amongst elemental mobility, Munsell color and low field mass normalized magnetic susceptibility (χ_{lf}). The study shows a consistent positive correlation of the rock magnetic parameters (principally magnetic susceptibility) with Munsell hue and Redness Rating (RR) index (Torrent et al., 1980, Blavet et al., 2000) of the soil profiles. The Late Miocene profiles show an increase of ~29% of Al_2O_3 concentration and that for the Pliocene and Pleistocene profiles show ~33 to 60% increase as a result of pedogenesis. Similarly the other immobile elemental oxide, Fe_2O_3 is increased by ~54% in the Late Miocene profiles and ~50 to ~63% in the Pliocene–Pleistocene profiles. Geochemical trends correlate with the χ_{lf}, showing $R^2 = 0.39$ to 0.68 with Al_2O_3 and Fe_2O_3 and $R^2 = -0.40$ to -0.73 for SiO_2. Similarly the Munsell color parameters, especially the RR index display significant positive correlation where the magnetic mineralogy is dominated by hematite and goethite. These first order relationships amongst χ_{lf}, RR index and elemental mobility demonstrate the potential use of magnetic susceptibility for rapid characterization of the widespread and heterogeneous pedogenic episodes within the dynamic sedimentary environments of the Himalayan foreland basin.

1. Introduction

The Late Cenozoic Siwalik sequence of the Himalayan Foreland Basin is the repository for a large variety of paleosols developed under varied climate, depositional and erosional conditions (Johnson, 1977; Willis and Behrensmeyer, 1995; Retallack, 1995; Zaleha, 1997; Thomas et al., 2002; Sangode and Bloemendal, 2004). These large number of paleosols demand attention to their characterization before attempting them for any major paleoclimatic and allostratigraphic study. Various methods including their field documentation and micromorphology can help to characterize these paleosols; however the truncated-, compound- and multistory-nature of these paleosols and their rapid lateral variations demands a suitable instrumental method for rapid characterization in agreement with field characteristics. This study presents an application of low field magnetic susceptibility to relate with the soil color and elemental mobility in some of the ideal sections of the Siwalik paleosol sequence in the NW Himalaya, India.

The low field magnetic susceptibility (χ_{lf}) is the most fundamental room temperature parameter forming the ratio of induced magnetization (I) to a weak applied field (H). It allows preliminary estimates on ferrimagnetic mineral contents (O'Reilly, 1984; Thompson and Oldfield, 1986). In sediments and mixtures, it varies with the proportionate variation in the ferri-, antiferro-, para-, and dia-magnetic material concentration besides their granulometry with various conditions described in Stacey and Banerjee (1974), O'Reilly (1984), Dunlop and Ozdemir (1997), Thompson and Oldfield (1986), Evans and Heller (2003).

Magnetic minerals (iron oxides and oxy-hydroxides) promptly response to the soil and water Eh–pH conditions, and can preserve perceptible first order information on the pedogenic processes (Torrent et al., 1980, 1983; Kampf and Schwertmann, 1983; Fitzpatrick, 1986; Torrent and Schwertmann, 1987; Singer et al., 1996; Torrent and Barrón, 2003). Soil formations under well drained aerobic conditions often enhance the susceptibility as a result of newly formed oxides of iron (Verosub et al., 1993; Singer et al., 1996; Maher, 1998; Evans and Heller, 2001). Ferrimagnetic minerals (magnetite and maghemite) are readily reducible and their dissolution can occur in poorly drained anoxic soil conditions lowering the magnetic susceptibility values as in the gleyed soils (Williams and Cooper, 1990; Williams, 1992; de Jong et al., 2000;

* Corresponding author. Fax: +91 20 25695373.
E-mail address: sangode@unipune.ernet.in (S.J. Sangode).

0016-7061/$ – see front matter © 2009 Elsevier B.V. All rights reserved.
doi:10.1016/j.geoderma.2009.10.013

Grimley and Vepraskas, 2000; Grimley et al., 2004; Hanesch and Scholger, 2005; Grimley and Arruda, 2007). Magnetic susceptibility changes in the soil/paleosols therefore can be related to pedogenic intensity, and based on susceptibility several quantifications are made as proxy to climatic variations (e.g. Mullins, 1977; Heller and Liu, 1984; Kukla et al., 1988; Fine et al., 1989, 1993; Maher and Thompson, 1992; Liu et al., 2007).

Magnetic susceptibility is one of the sensitive and most readily reproducible parameters although it is crucial to find the source of magnetic susceptibility signals especially in the polyphase (/multi-mineral) pedofacies such as the Siwalik paleosols. It is therefore necessary to integrate the magnetic susceptibility results with other dependant and independent parameters like rock magnetism, elemental mobility and field characters like the soil color.

The soil color is principally governed by the mineral forms like iron oxides (e.g. hematite and goethite), Fe–Mn oxides, humic substances (Plice, 1942, 1945; Schwertmann, 1993; Torrent and Barrón, 1993; Scheinost and Schwertmann, 1999) and clay minerals. Hematite generally produces reddish brown color and various shades of yellowish brown are often imparted by limonite and goethite (Plice, 1942; Torrent

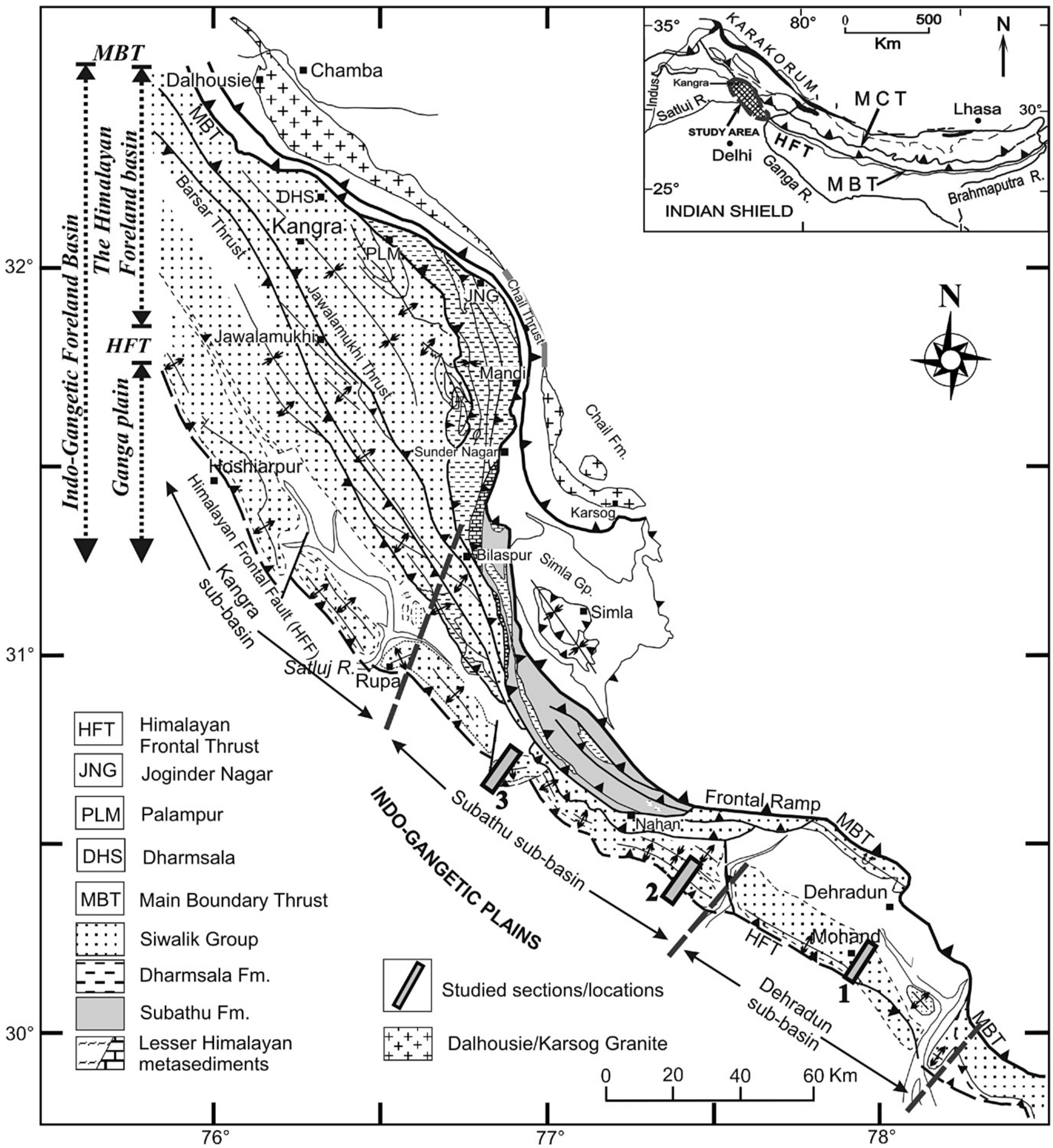

Fig. 1. The geological map of the study area showing the locations of the studied sections (compiled from Karunakaran and Rao, 1976; Thakur, 1998; Valdiya, 1998). 1. Mohand Rao, 2. Haripur Khol and 3. Ghaggar section. The Haripur Khol and Ghaggar sections are from the Subathu sub-basin that comprises essentially of Upper Siwalik sequences. The Mohand Rao section constitutes Middle and Upper Siwalik sediments and situated in the Dehra Dun sub-basin.

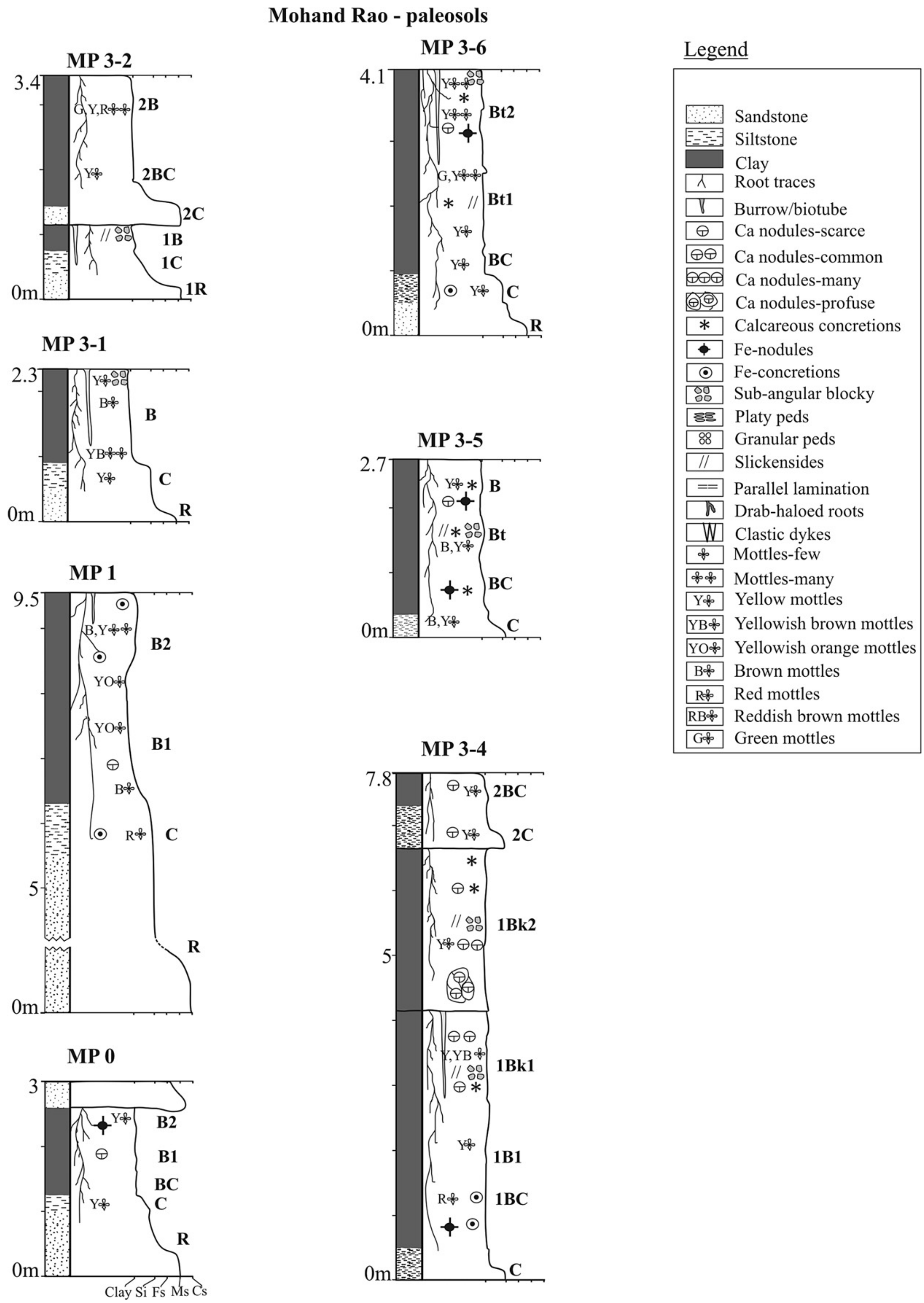

Fig. 2. Detailed lithologs of the representative paleosol profiles from MR, HK and GH sections are showing macroscopic pedogenic features of each horizon.

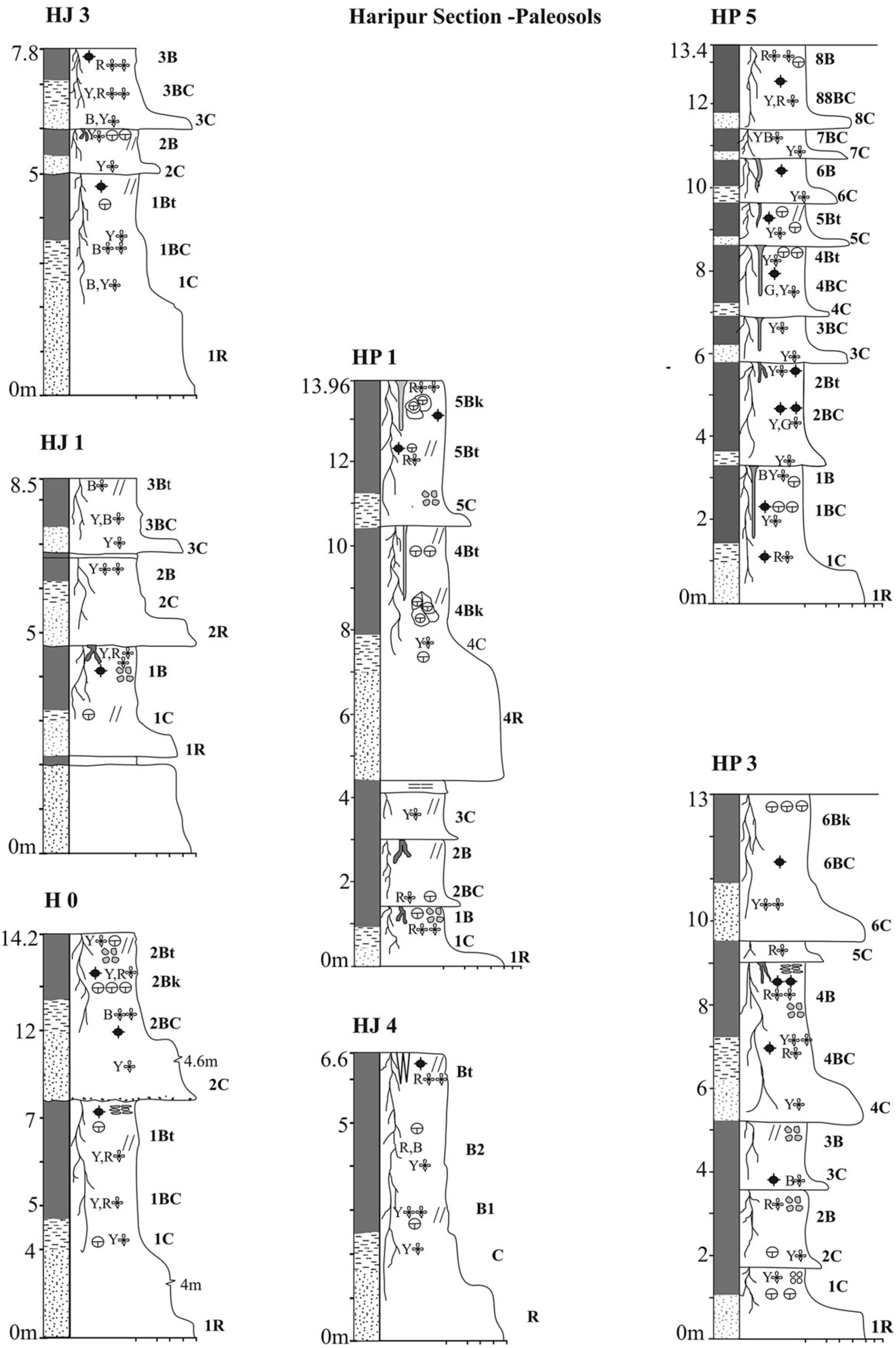

Fig. 2 (*continued*).

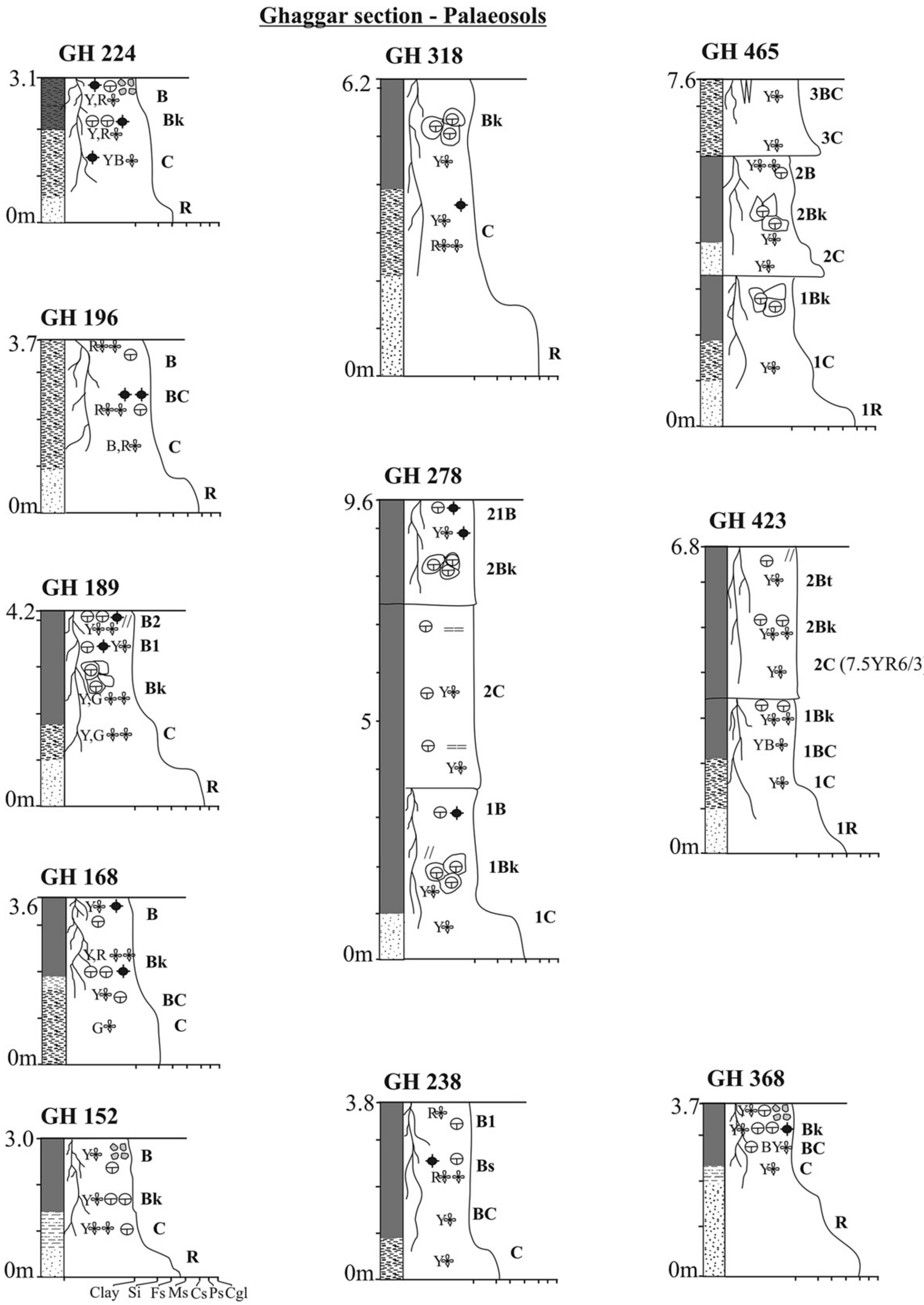

Fig. 2 (*continued*).

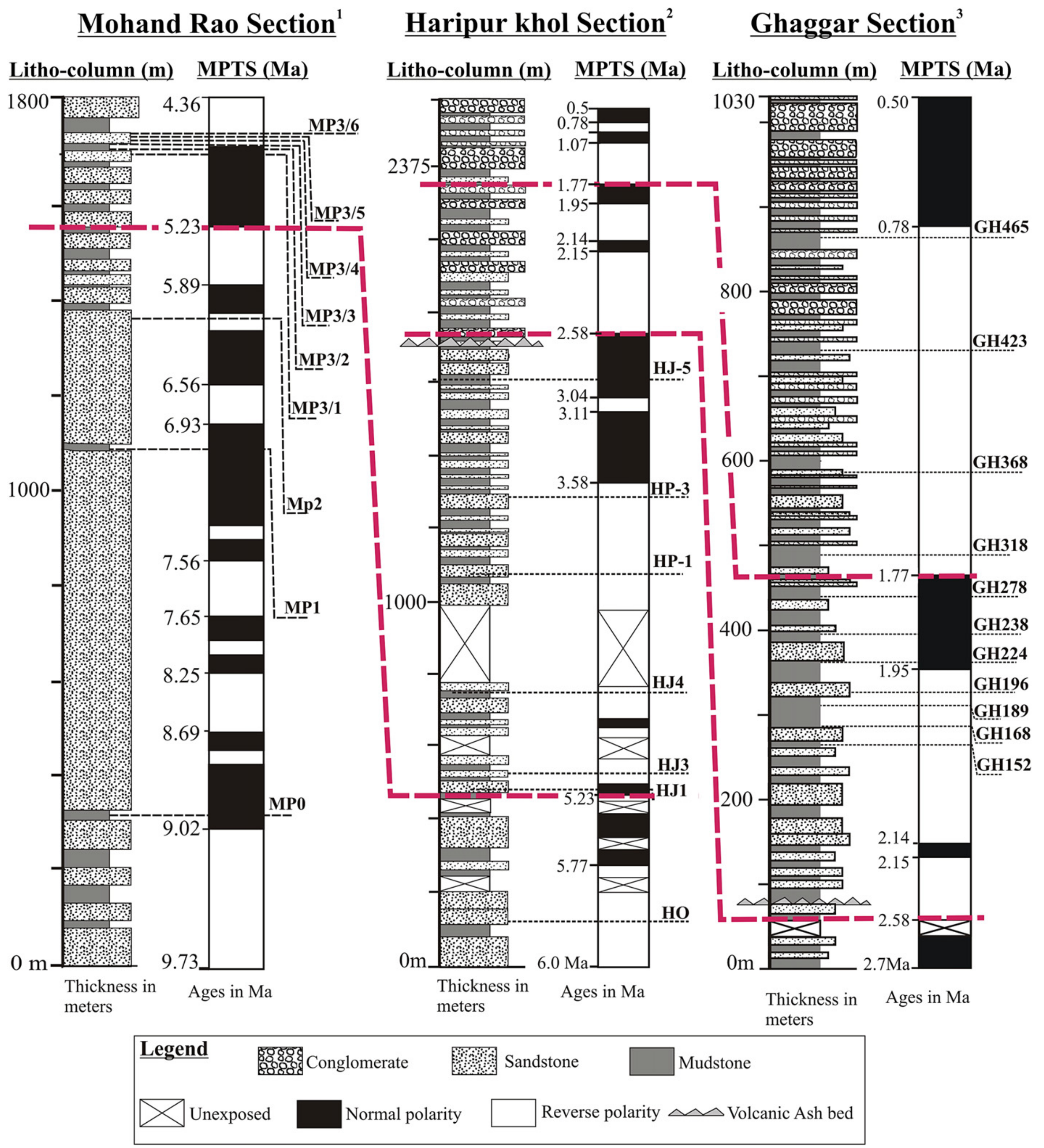

Fig. 3. Lithostratigraphy and magnetostratigraphy of the studied sections showing the stratigraphic position of each paleosol profile. Magnetostratigraphic ages are established by [1]Sangode et al. (1999), [2]Sangode et al., (1996) and [3]Kumaravel et al. (2005a). Broken red lines are correlating the similar age zones among sections. (For interpretation of the references to color in this figure legend, the reader is referred to the web version of this article.)

et al., 1980, 1983; Barrón and Torrent, 1987; Torrent and Schwertmann, 1987). The Munsell notation (Munsell, 2000) being an alphanumeric index, it is not readily reproducible for correlation to other independent parameters like susceptibility and geochemical indices. Torrent et al. (1983) and Torrent and Schwertmann (1987) developed a quantitative relationship between soil color and hematite content from different geographic locations developing the redness rating index. Recently, Blavet et al. (2000) developed an empirical relation to quantify the angular hue. Torrent and Barrón (2003) further reviewed the relationship of iron oxides with color for the Mediterranean soils. However, the studies relating the soil color with mineral magnetic parameters especially with magnetic susceptibility are still awaited. We therefore attempt here to investigate the relation between magnetic susceptibility and soil color with the help of the geochemical parameters. The results are based on combined analysis of mineral magnetism, Munsell color notations and major element geochemistry of 27 paleosol profiles from three magnetostratigraphically constrained sections of the Middle and Upper Siwalik fluvial sections namely Mohand Rao (MR), Haripur Khol (HK) and Ghaggar river (GH) (see Fig. 1). Litho-logs of the representative paleosol profiles are produced in Fig. 2 and their stratigraphic position and magnetostratigraphic ages are seen in Fig. 3.

2. Samples and methods

A total of 213 samples (147 pedogenic horizons and 66 parent/bedrocks) were collected from three stratigraphic columns shown in Figs. 2 and 3. The MR section is about 1800 m thick with the lower 1400 m part comprising of Middle Siwalik that shows thickly bedded gray-, friable-, salt and pepper sandstones in multi-storey geometry with occasional lenses of mudstones and few occurrences of moderately developed paleosols. The upper part of this section (*i.e.*, 1440–1800 m interval) display fine- to coarse grained multistoried sandstones and mudstones with frequent occurrence of pedogenic layers (Fig. 3). Total 9 clear paleosol profiles (denoted as MP 0, MP 1, MP 2, MP 3-1, MP 3-2, MP 3-3, MP 3-4, MP 3-5 and MP 3-6) from the MR section were undertaken for the present study (Figs. 2 and 3). Similarly a total of 7 paleosol profiles (H 0, HJ 1, HJ 3, HJ 4, HP 1, HP 3 and HP 5) are selected from the ~2375 m thick HK section (Figs. 2 and 3) comprising Middle Siwalik (Dhok Pathan Formation) and Upper Siwalik (Tatrot, Pinjor and Boulder Conglomerate) formations. The Dhok Pathan Formation of the HK section characterizes thickly bedded gray multistoried sandstones and rare overbank mudstones. The overlying Tatrot and Pinjor Formations essentially consist of ribbon shaped gray and buff sandstones with variegated mudstones. The succeeding Boulder Conglomerate Formation comprises thickly bedded massive to stratified conglomerates with few lensoid mudstone intervals. The Ghaggar section represents 1030 m thick Upper Siwalik sequences (Tatrot, Pinjor and Boulder Conglomerate formations). A total of 11 paleosol profiles (GH 152, GH 168, GH 189, GH 196, GH 224, GH 238, GH 278, GH 318, GH 368, GH 423 and GH 465) from this section are studied (Fig. 3).

Brown to grayish brown- fine-, medium- and coarse grained sandstone, multistoried sandstones, pedogenic and non-pedogenic mudstones are abundant in both the Tatrot and Pinjor Formation. The Boulder Conglomerate Formation consists of thickly bedded massive conglomerates with interstratified sandstone and mudstones and infrequent truncated paleosols. Detailed sedimentological studies including facies association, sediment architecture, paleoflow, petro-mineralogy, grainsize and clay mineralogy, magnetostratigraphy, rock magnetism and their climatic and tectonic inferences for the above sections are given in Kumar and Tandon (1985), Kumar (1993), Sangode et al. (1999), Thomas et al. (2002), Kumar et al. (2003, 2004), Sangode and Bloemendal (2004), Siddaiah and Sangode (2005), Kumaravel et al. (2005a,b, 2009).

Samples for magnetic properties were prepared in standard non-magnetic (styrene) 10 cm^3 cylindrical pots and measured using Bartington magnetic susceptibility meter (MS 2B) for low and high frequency (0.465 kHz and 4.65 kHz) of applied fields. Percentage of frequency dependent susceptibility (χ_{fd}%) has been calculated from the low (χ_{lf}) and high (χ_{hf}) frequency values $\{(\chi_{lf}-\chi_{hf})/(\chi_{lf})\times 100\}$. Magnetic mineralogy for these paleosols is described in details in Sangode and Bloemendal (2004), Kumaravel et al. (2005b) and Sangode et al. (2008).

For major element analysis the paleosol samples were powdered to <74 μm in the agate Tima Mill. Standard pellets were prepared out of 5 g of homogenized samples for the X-Ray Fluorescence Spectrometry analysis (using Siemens, SRS3000 XRF system). Major oxides (SiO_2, Al_2O_3, Fe_2O_3, Na_2O, MgO, CaO, K_2O, MnO, P_2O_5, and TiO_2) were analyzed against USGS standard (GXR-1, SCo-1, SDO-1 and SGR-1) with a precision better than 1.5%.

Depletion of soluble elements in pedogenic layers with respect to the parent material are determined by using the equation;

$$\text{Elemental depletion\%} = \frac{(\text{mean parent wt.\%} - \text{mean pedogenic wt.\%})}{\text{mean parent wt.\%}} \times 100$$

The elemental enrichment due to pedogenesis is determined as below;

$$\text{Elemental enrichment\%} = \frac{(\text{mean pedogenic wt.\%} - \text{mean parent wt.\%})}{\text{mean parent wt.\%}} \times 100$$

Munsell color of the paleosol samples was noted in field by digging fresh surface at each location. However since the incident light and moisture conditions vary at each location in the incised sections, we followed a laboratory method where 20 g of the disaggregated and homogenized sample was dissolved in distilled water and exposed to natural daylight under uniform laboratory conditions to note the Munsell color. The Redness Rating (RR) is calculated from the Munsell color notations following the expression given in Torrent et al. (1980) as below;

$$RR = \frac{H \times C}{V}$$

Where, H is the numerical value of Munsell hue assigned as 7.5 for 2.5YR; 5 for 5YR; 2.5 for 7.5YR; 0 for 10YR; −2.5 for 2.5Y and −5 for 5Y; V and C are numerical values of Munsell 'Value' and 'Chroma', respectively.

3. Results and discussion

3.1. Mohand Rao (MR) paleosols

The mean χ_{lf} calculated for all the C-horizons is ~$7.3\times10^{-9}\,m^3\,kg^{-1}$ while that for the paleosols shows ~30% increase with a mean value of ~$9.5\times10^{-9}\,m^3\,kg^{-1}$ (Fig. 4). The rock magnetic studies of the MR section paleosols infer an overall predominance of the antiferro-magnetic minerals (*e.g.* goethite and hematite; Kumaravel et al., 2005b). Very high values for coercivity of remanence (B_{0CR}) of the order of ~600 mT with mean of 425 mT indicate the enrichment of the hard magnetic minerals in these paleosols (Kumaravel et al., 2005b). The color of the paleosols varies from reddish brown (5YR 4/3) to strong brown (7.5YR 4/6). The χ_{lf}, χ_{fd}%, Munsell notation, and sampling depth for each pedogenic horizon are produced in Table 1. Although these paleosols contain significant amount of iron oxides (hematite and goethite), the susceptibilities are lower due to antiferromagnetic nature

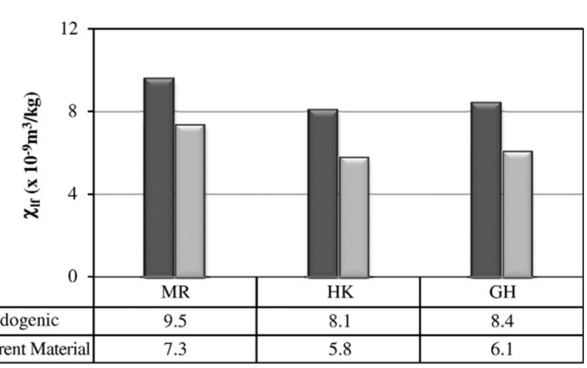

Fig. 4. Bar diagram illustrates the amplification of magnetic susceptibility signal for the MR, HK and GH paleosols due to pedogenesis. The χ_{lf} is increased by 30% in the MR paleosols while it is 40% and 39% for HK and GH paleosols, respectively. This indicates the significant increment of the concentration of magnetic minerals in the paleosols as a result of soil forming processes.

Table 1
Munsell color notation, sampling height, redness rating and low field and frequency dependent magnetic susceptibility of pedogenic horizons of MR, HK and GH paleosols.

S. no.	Sample no.	Stratigraphic height (m)	Sampling height (m)	Color (Munsell)	RR index	χ_{lf} ($\times 10^{-9}$ m^3/kg)	χ_{fd}%
1	MPL0-1B1	330	1.38	7.5YR 5/6	3.0	9.8	5.5
2	MPL0-1B2		1.55	10YR 6/6	0.0	6.9	5.0
3	MPL0-1B3 L		1.87	7.5YR 5/4	2.0	9.7	0.0
4	MPL0-1B3U		2.08	7.5YR 6/4	1.7	11.1	2.5
5	MPL0-1B4		2.40	7.5YR 6/6	2.5	10.4	0.0
6	MPL1-1C	1080	5.90	7.5YR 5/6	3.0	11.5	0.0
7	MPL1-1B1		6.68	7.5YR 4/3	1.9	7.8	0.0
8	MPL1-1B2		7.30	7.5YR 4/4	2.5	5.5	0.0
9	MPL1-1B3		7.80	7.5YR 4/6	3.8	6.3	0.0
10	MPL1-1B4		8.30	10YR 5/4	0.0	5.0	0.0
11	MPL1-1B5		8.80	10YR 5/6	0.0	6.5	5.4
12	MPL1-1B6		9.30	10YR 5/4	0.0	6.9	0.0
13	MPL2-1C L	1390	0.63	7.5YR 4/3	1.9	8.6	5.3
14	MPL2-1CU		0.83	10YR 4/1	0.0	8.6	0.0
15	MPL2-B1 L		1.15	7.5YR 5/3	1.5	10.8	5.4
16	MPL2-B1 U		1.45	7.5YR 4/3	1.9	9.6	3.1
17	MPL3-1B1	1750	1.05	7.5YR 5/4	2.0	11.3	1.4
18	MPL3-1B2		1.43	7.5YR 4/2	1.3	11.8	0.0
19	MPL3-1B3		1.88	5YR 4/2	2.5	11.1	2.4
20	MPL3-1B4		2.28	7.5YR 3/2	1.7	10.7	0.0
21	MPL3-2C	1753	0.68	2.5Y 4/1	−0.6	10.6	4.8
22	MPL3-2B1		0.95	10YR 5/8	0.0	11.0	0.0
23	MPL3-2B2 L		1.85	2.5YR 4/3	5.6	9.3	3.0
24	MPL3-2B2 U		2.40	5YR 4/3	3.8	9.3	0.0
25	MPL3-2B3 L		2.88	7.5YR 6/6	2.5	10.0	2.8
26	MPL3-2B3 U		3.28	5YR 5/6	6.0	11.1	1.3
27	MPL3-3B1	1757	1.40	7.5YR 5/4	2.0	8.2	0.0
28	MPL3-3B2		2.08	7.5YR 4/4	2.5	13.6	8.3
29	MPL3-4B1	1760	1.30	7.5YR 5/8	4.0	9.0	1.8
30	MPL3-4B2		1.90	7.5YR 5/6	3.0	10.7	1.9
31	MPL3-4B3		2.50	10YR 5/6	0.0	7.8	2.2
32	MPL3-4B4		3.23	2.5Y 6/4	−1.7	9.0	5.3
33	MPL3-4B5A		3.90	5YR 4/3	3.8	11.5	5.4
34	MPL3-4B5B		4.53	5YR 4/4	5.0	9.6	0.0
35	MPL3-4B5C		5.03	5YR 3/3	5.0	10.1	0.0
36	MPL3-4B5D		5.35	5YR6/6	5.0	10.1	4.1
37	MPL3-4B5E		5.73	5YR 5/6	6.0	10.2	1.5
38	MPL3-4B5F		6.13	5YR 6/6	5.0	10.5	0.0
39	MPL3-4B5G		6.50	5YR 5/4	4.0	10.0	6.2
40	MPL3-4B6		6.85	5YR 4/3	3.8	6.8	0.0
41	MPL3-4B7		7.18	7.5YR 4/6	3.8	10.0	0.0
42	MPL3-4B8		7.55	5YR 4/6	7.5	9.6	3.3
43	MPL3-5B1	1768	1.63	7.5YR 5/4	2.0	7.9	0.0
44	MPL3-5B2		2.10	10YR 4/3	0.0	9.3	3.5
45	MPL3-5B3		2.48	5YR 4/4	5.0	10.1	1.3
46	MPL3-6B1	1771	1.13	5YR 4/4	5.0	10.7	3.1
47	MPL3-6B2		1.55	5YR 5/6	6.0	11.0	3.8
48	MPL3-6B3		1.80	7.5YR 4/6	3.8	10.3	1.4
49	MPL3-6B4		2.10	7.5YR 5/4	2.0	9.7	11.1
50	MPL3-6B5		2.40	7.5YR 5/6	3.0	9.1	0.0
51	MPL3-6B6		2.70	7.5YR 5/8	4.0	9.2	0.0
52	MPL3-6B7		3.05	7.5YR 5/8	4.0	8.2	0.0
53	MPL3-6B8		3.35	10YR 6/6	0.0	8.7	0.0
54	MPL3-6B9		3.63	7.5YR 4/6	3.8	10.1	1.9
55	MPL3-6B10		3.93	10YR 4/4	0.0	10.2	0.0
Haripur paleosols							
56	HJ1/B1	485	3.40	7.5YR 4/3	1.9	9.3	3.3
57	HJ1/B2		3.75	5YR 4/4	5.0	6.4	4.2
58	HJ1/B3		4.05	7.5YR 4/6	3.8	6.6	4.4
59	HJ1/B4		4.50	5YR 3/3	5.0	11.3	2.2
60	HJ1/1B1		6.50	10YR 4/3	0.0	6.5	2.3
61	HJ1/2B1		7.80	7.5YR 4/4	2.5	7.6	2.5
62	HJ1/2B2-L		8.20	5YR 3/3	5.0	10.1	0.4
63	HJ3/1B1	534	3.35	7.5YR 4/4	2.5	4.7	2.3
64	HJ3/1B2-L		3.90	7.5YR 5/4	2.0	7.8	0.0
65	HJ3/1B2-U		4.10	7.5YR 4/3	1.9	8.1	0.5
66	HJ3/1B3-L		4.50	7.5YR 5/2	1.0	8.0	0.3
67	HJ3/1B3-U		4.80	7.5YR 4/2	1.3	11.5	1.4
68	HJ3/2B1-L		5.50	7.5YR 4/3	1.9	9.6	2.7
69	HJ3/2B1-M		5.70	7.5YR 5/4	2.0	8.5	2.5
70	HJ3/2B1-U		5.90	5Y 4/3	−3.8	5.6	1.8
71	HJ4/B1	752	2.80	7.5YR 4/6	3.8	8.9	0.0
72	HJ4/B2-L		3.40	7.5YR 4/6	3.8	6.6	1.0
73	HJ4/B3		4.45	7.5YR 4/4	2.5	6.0	1.1

Table 1 (*continued*)

S. no.	Sample no.	Stratigraphic height (m)	Sampling height (m)	Color (Munsell)	RR index	χ_{lf} ($\times 10^{-9}$ m^3/kg)	χ_{fd}%
74	HJ4/B4		5.05	7.5YR 4/3	1.9	6.2	1.6
75	HJ4/B5-U		5.90	10YR 5/6	0.0	5.9	0.4
76	HJ4/B6-L		6.30	7.5YR 5/6	3.0	6.6	0.6
77	HJ4/B6-U		6.50	7.5YR 4/3	1.9	9.6	0.3
78	HPL 1/B1	1077	1.25	7.5YR 5/8	4.0	7.2	1.3
79	HPL 1/B2-L		1.70	2.5Y 5/4	−2.0	8.2	0.0
80	HPL 1/B2-U		2.10	2.5Y 5/4	−2.0	8.5	0.0
81	HPL 1/B3		2.70	2.5Y 6/4	−1.7	7.9	0.0
82	HPL 1A/B1		8.30	7.5YR 4//4	2.5	9.4	3.4
83	HPL 1A/B2		9.30	7.5YR 5/6	3.0	9.3	0.0
84	HPL 1A/B3		10.15	7.5YR 4/6	3.8	9.6	11.7
85	HPL 1A/B4		10.85	7.5YR 5/8	4.0	5.8	4.4
86	HPL 1A/B5		11.50	7.5YR 5/6	3.0	9.7	2.2
87	HPL 1A/B6-L		12.00	2.5Y 6/6	−2.5	8.7	1.0
88	HPL 1A/B6-U		12.30	10YR 6/6	0.0	8.1	1.9
89	HPL 1A/B7		12.85	5YR 5/6	6.0	10.3	2.0
90	HPL 1A/B8		13.45	10YR 6/6	0.0	8.3	0.0
91	HPL3 1A/B2	1294	3.05	7.5YR 4/4	2.5	10.9	1.5
92	HPL3 1B/C		4.85	2.5Y 5/4	−2.0	9.6	0.0
93	HPL3 1C/C		6.90	10YR 5/4	0.0	7.7	1.6
94	HPL3 1C/B1		7.75	10YR 6/8	0.0	10.0	0.0
95	HPL3 1C/B2		8.40	2.5Y 6/3	−1.3	4.5	0.0
96	HPL3 1C/B3		8.85	7.5YR 4/6	3.8	10.6	0.5
97	HPL3 1D/C		11.25	2.5Y 6/4	−1.7	7.1	1.8
98	HPL3 1D/B1		12.25	10YR 5/4	0.0	8.9	1.1
99	HPL5 1/B1-L	1602	2.70	10YR 4/4	0.0	7.3	7.6
100	HPL5 1/B1-U		2.85	10YR 4/3	0.0	7.9	2.6
101	HPL5 1/B2		3.15	2.5Y 5/4	−2.0	7.9	0.0
102	HPL5 1/B3		3.70	7.5YR 4/3	1.9	10.5	2.1
103	HPL5 1/B4-L		4.35	2.5Y 6/6	−2.5	6.3	2.6
104	HPL5 1/B4-U		4.75	2.5Y 6/4	−1.7	5.7	0.0
105	HPL5 1/B5		5.40	10YR 5/4	0.0	8.2	0.0
106	HPL5 1A/C		6.75	10YR 5/3	0.0	9.9	2.4
107	HPL5 1B/C		7.50	10YR 4/3	0.0	9.1	0.6
108	HPL5 1B/B1		7.95	10YR 4/6	0.0	7.4	0.2
109	HPL5 1B/B2		8.40	7.5YR 4/6	3.8	9.8	1.8
110	HPL5 1C/C		9.10	10YR 5/4	0.0	6.9	1.3
111	HPL5 1C/B1		9.45	7.5YR 4/4	2.5	8.8	0.0
112	HPL5 1D/C		10.45	10YR 5/4	0.0	8.0	2.1
113	HPL5 1E/C		11.25	10YR 4/4	0.0	6.9	0.0
114	HPL5 1F/C		12.45	2.5Y 5/4	−2.0	6.6	0.0
115	HPL5 1F/B1		13.05	5Y 6/4	−3.3	6.8	0.8
Ghaggar paleosols							
116	GH152/B1	264	1.65	2.5Y 5/4	−2.0	6.0	0.0
117	GH152/B2		2.50	10YR 4/3	0.0	19.2	7.4
118	GH168/B1	285	2.20	10YR 5/6	0.0	10.2	0.0
119	GH168/B2		3.10	10YR 5/4	0.0	29.7	8.1
120	GH189/B1-M	310	2.70	10YR 6/6	0.0	6.4	1.8
121	GH189/B2		3.50	10YR 5/6	0.0	5.7	1.5
122	GH189/B3		3.95	2.5Y 6/4	−1.7	7.9	1.5
123	GH196/B1	326	2.40	10YR 6/6	0.0	5.5	0.0
124	GH196/B2		3.20	10YR 5/4	0.0	8.4	5.7
125	GH224/B1	361	2.25	10YR 5/8	0.0	6.6	0.0
126	GH224/B2		2.80	2.5Y 6/6	−2.5	7.4	1.1
127	GH238/C	394	1.40	7.5YR 5/6	3.0	9.2	1.6
128	GH238/B1-M		2.45	10YR 5/6	0.0	7.8	2.9
129	GH238/B2		3.20	10YR 4/4	0.0	10.4	2.0
130	GH278/B1-M	438	3.05	10YR 5/4	0.0	10.8	1.4
131	GH278/B3		5.50	7.5YR 4/4	2.5	12.8	4.0
132	GH278/B5		8.05	7.5YR 5/6	3.0	8.1	0.0
133	GH278/B6-U		9.10	7.5YR 5/8	4.0	6.5	3.3
134	GH278/B7		9.45	10YR 6/8	0.0	6.5	1.6
135	GH318/B1-U	488	4.30	7.5YR 5/6	3.0	11.0	2.7
136	GH318/B2		5.35	7.5YR 4/3	1.9	8.3	0.0
137	GH368/B1	586	2.65	7.5YR 5/6	3.0	6.1	0.0
138	GH368/B2		3.15	10YR 6/6	0.0	7.4	0.6
139	GH368/B3		3.55	10YR 6/4	0.0	7.6	0.0
140	GH423/B2	730	3.15	10YR 5/6	0.0	6.9	1.3
141	GH423/1C		4.05	7.5YR 4/4	2.5	7.9	0.6
142	GH423/1B1		5.00	7.5YR 4/4	2.5	9.0	0.0
143	GH423/1B2		6.05	7.5YR 5/4	2.0	10.3	0.0
144	GH465/B1	863	2.70	10YR 6/6	0.0	4.4	0.3
145	GH465/1B1		4.20	10YR 5/4	0.0	9.1	2.2
146	GH465/1B3		5.50	10YR 6/4	0.0	25.3	6.0
147	GH465/2B1		7.20	10YR 5/4	0.0	26.5	5.3

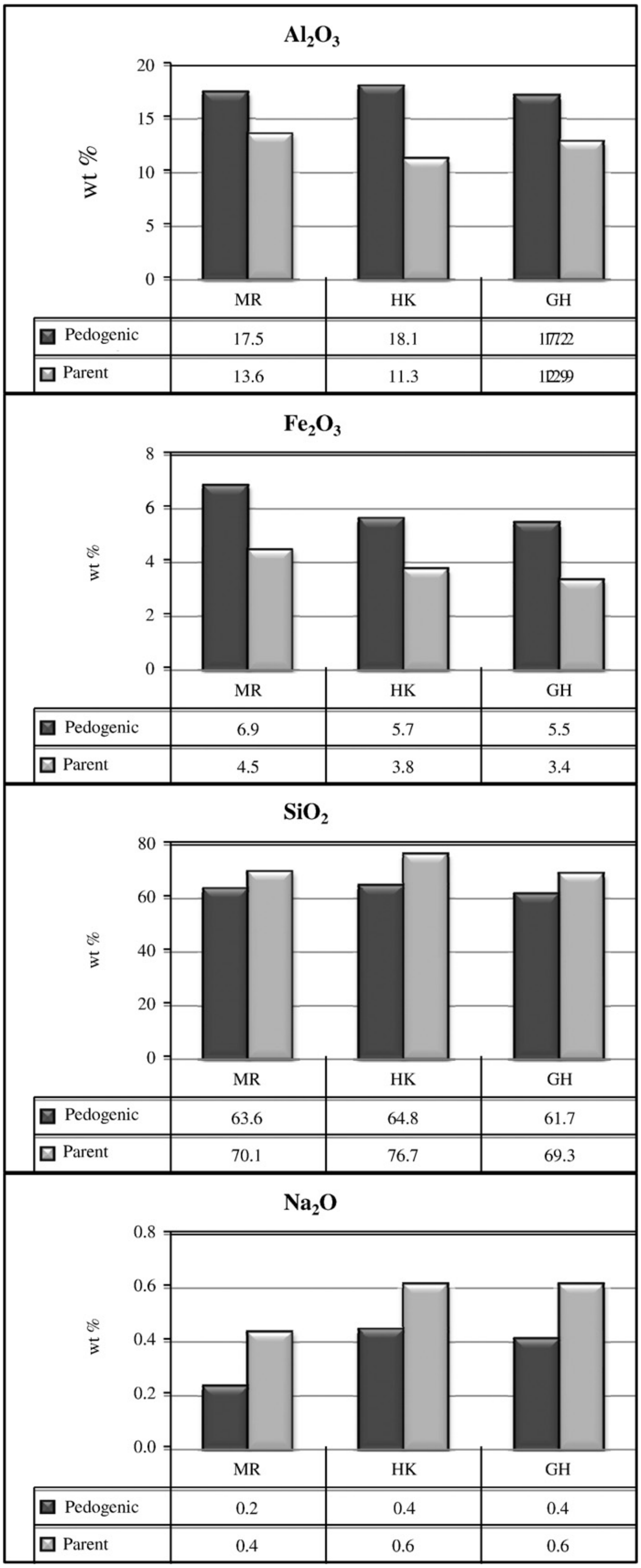

Fig. 5. Bar diagram represents the relative increase or decrease of the significant geochemical parameters of the MR, HK and GH paleosols, with reference to corresponding parent material, as a result of pedogenesis.

of the minerals (hematite and goethite). However, the susceptibility measurements are notably consistent with high repeatability each specimen on the Bartington unit (MS 2B sensor).

The most stable elemental oxides Al_2O_3 and Fe_2O_3 increase exponentially from 13.6 wt.% and 4.5 wt.% in the parent to 17.5 wt.% and 6.9 wt.% in the pedogenic horizons (Fig. 5). Overall, the pedogenic horizons witness about 29% and 54% increases in Al_2O_3 and Fe_2O_3, respectively (Fig. 6). Similarly, the pedogenic horizons show depletion of the base cations (mean wt.% of $Na_2O = 0.24$, $CaO = 0.51$, $SiO_2 = 63.6$) compared to their enrichment in the parents ($Na_2O = 0.44$; $CaO = 1.3$; $SiO_2 = 70.1$) (see Fig. 5). The Na_2O is depleted to the extent of 46% while SiO_2 is depleted to about 9% as a result of pedogenesis (Fig. 6).

3.2. Haripur Khol (HK) paleosols

The pedogenic horizons of the HK paleosols show mean χ_{lf} of ~8.1 ($\times 10^{-9}\,m^3\,kg^{-1}$) with that for the associated parent material of ~5.8 ($\times 10^{-9}\,m^3\,kg^{-1}$) (Fig. 4). This accounts for about 40% enhancement of the magnetic susceptibility in the pedogenic layers (Fig. 4). The detailed rock magnetic investigation on Haripur (HK) paleosols by Sangode and Bloemendal (2004) inferred high coercivity of remanence (mean $B_{0CR} = 447$ mT) and the high mean hysteresis ratio (mean Mrs/Ms = 0.6) due to predominance of the imperfect and canted antiferromagnetic minerals (hematite and goethite). The HK paleosols are characteristic of dark reddish brown (5YR 3/3), brown (7.5YR 5/4) to yellowish brown (10YR 5/6) color of pedogenic layers.

Al_2O_3 concentrations in the pedogenic layers are increase by 18.1 (mean wt.%) compared to the substratum that shows 11.3 mean wt.% (see Fig. 5). The percentage increase in Al_2O_3 content is as high as 60% as a result of illuviation and eluviation during pedogenesis (Fig. 6). The Fe_2O_3 is also increased in the pedogenic layers (mean wt.% of $Fe_2O_3 = 5.7$) by about 50% with respect to the corresponding parent material (mean wt.% of $Fe_2O_3 = 3.8$). The base cations (e.g. Na_2O) and silica (SiO_2) that are soluble during pedogenesis are leached out and are depleted in the pedogenic layers. The SiO_2 content in the HK paleosols are reduced to about 16% (mean wt.% = 65) in contrast to the respective parent materials that shows SiO_2 mean wt.% of 77 (see Fig. 5). However, the net increase in the MgO (1.37 to 1.83 wt.%) in the paleosols could be explained by the dolomitization during or after the formation of the paleosols.

3.3. Ghaggar Section (GH) paleosols

The GH paleosols show about 39% increase in magnetic susceptibility in the soil solum compared to the parental sandstone and mudstones (Fig. 4). These paleosols are typically yellowish brown (10YR 5/6) to brownish yellow (10YR 6/6) in color. The concentration of immobile elements in these paleosols is 17.2 and 5.5 mean wt.% of Al_2O_3 and Fe_2O_3, respectively, compared to their lower percentage of 12.9 and 3.4 in the parent material. The Al_2O_3 and Fe_2O_3 shows about 33% and 63% increase, respectively in the paleosols compared to parent suggesting the accumulation of sesquioxides during to pedogenesis (Fig. 6). The base cations (mean wt.% of $Na_2O = 0.62$; $CaO = 2.63$) and silica (mean $SiO_2 = 69.3$ wt.%) are found to be relatively abundant in the parent compared to the paleosols (mean wt.% of $Na_2O = 0.41$; $CaO = 1.94$; $SiO_2 = 61.7$) (see Fig. 5). The leaching of Na_2O (33%) and SiO_2 (11%) indicate the activeness of dissolution processes during pedogenesis (Fig. 6).

4. Pedogenic relation of magnetic and geochemical parameters

Amongst the three studied sections, HK paleosols (~6.0 Ma to 2.5 Ma) shows the largest increase in susceptibility (~40%), Al_2O_3 and Fe_2O_3 wt.% (60% and 50%, respectively) due to pedogenesis (Fig. 6). This increase is reasonably higher compared to the paleosols from the MR and GH sections. It infers that the HK paleosols are comparatively more strongly developed with their degree of pedogenesis higher than the MR and GH paleosol profiles. The higher pedogenic intensity

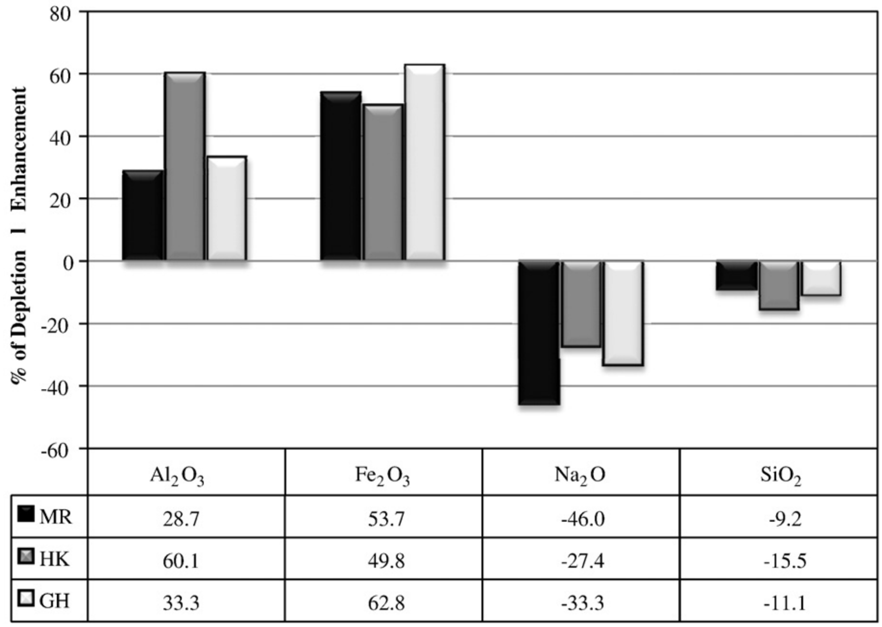

Fig. 6. Bar diagram depicts the enhancement percentage of Al_2O_3 & Fe_2O_3 and depletion percentage of SiO_2 & Na_2O, with respect to the corresponding parent material. The Al_2O_3 is increased up to 60% in the HK paleosols while GH paleosols records the highest increment of Fe_2O_3 of 63%.

amongst HK paleosols may be attributed to the upland depositional setup for this area (Thomas et al., 2002 and Kumar et al., 2003).

Overall the detailed comparison of the studied profiles in all the sections shows sensible relation of χ_{lf} with elemental mobility (Figs. 7 and 8). To summarize, the χ_{lf} of MR, HK and GH paleosols show consistently positive correlation with Al_2O_3 (MR = 0.56; HK = 0.68; GH = 0.39) and Fe_2O_3 (MR = 0.56; HK = 0.65; GH = 0.45) and negative correlation with SiO_2 (MR = −0.52; HK = −0.73; GH = −0.40; see Fig. 7). Thus the magnetic susceptibility variation is compatible with the elemental mobility and hence pedogenesis.

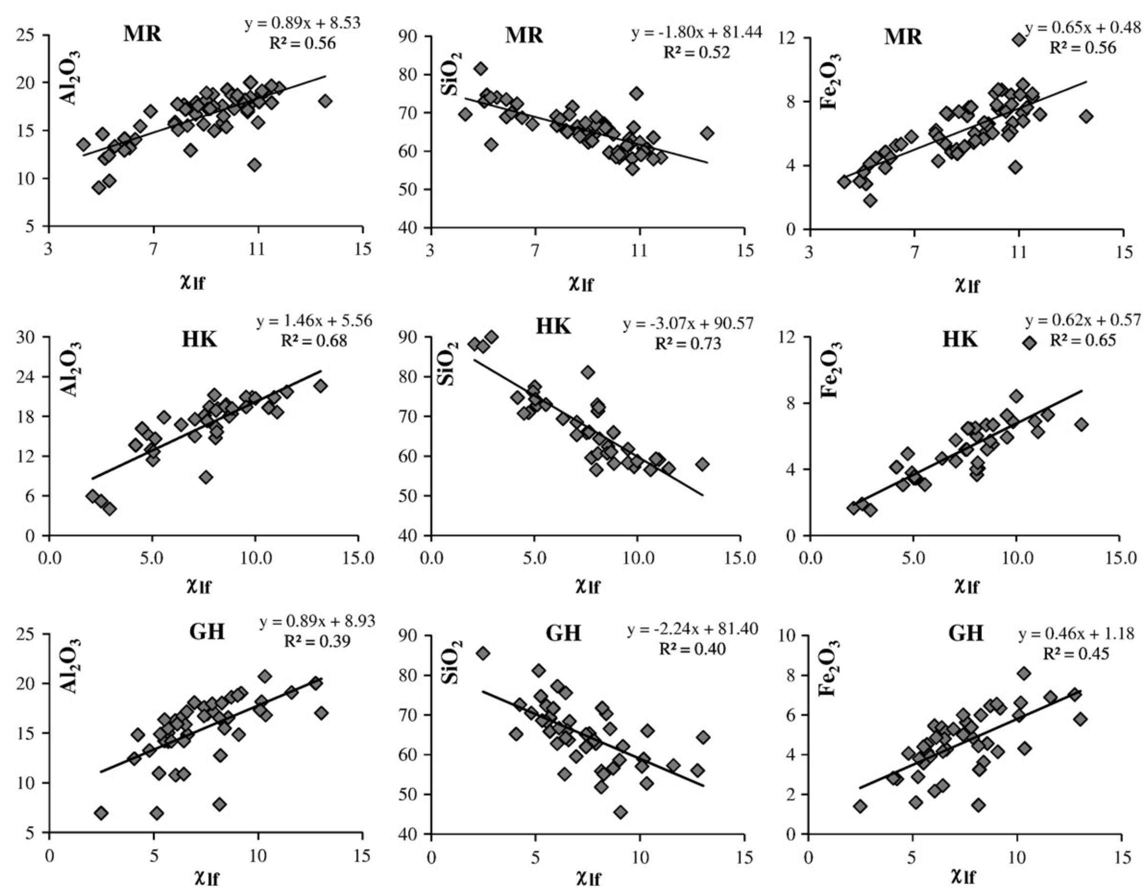

Fig. 7. Bivariate plots showing the relation of magnetic susceptibility with geochemical parameters of MR, HK and GH paleosols. The χ_{lf} ($\times 10^{-9} m^3 kg^{-1}$) shows positive correlation with Al_2O_3 (wt.%) and Fe_2O_3 (wt.%) while SiO_2 (wt.%) exhibits negative relationship.

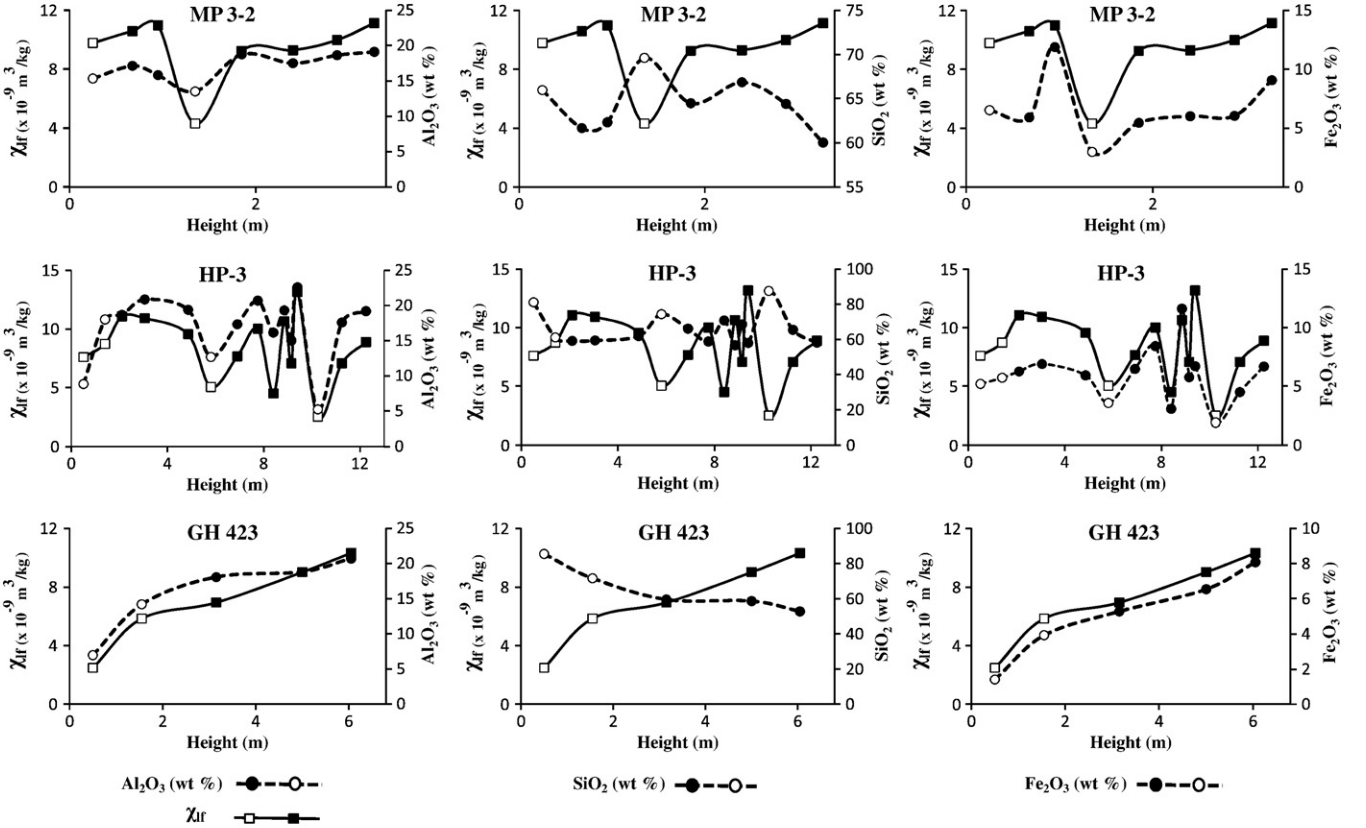

Fig. 8. Bivariate plots of χ_{lf} and Al_2O_3, Fe_2O_3 and SiO_2 vs. height of representative profiles from MR (MP 3-2), HK (HP3) and GH (GH423) paleosols showing the mutual behavior of χ_{lf} and geochemical parameters. Open circles and squares represent parent samples; filled circles and squares represent pedogenic samples.

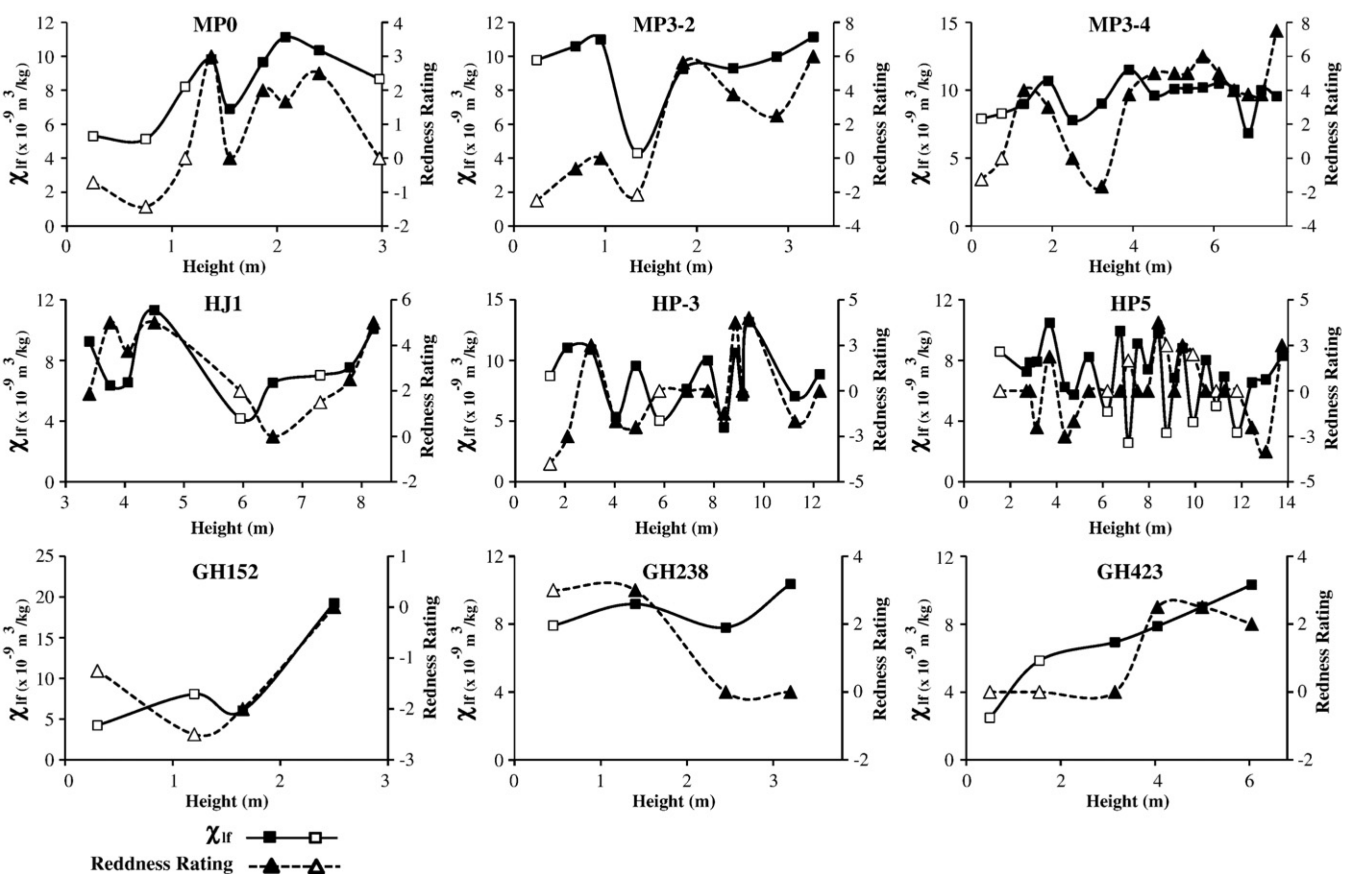

Fig. 9. Bivariate plots of χ_{lf} along with RR index vs. height of representative profiles from MR, HK and GH paleosols showing parallelism between the χ_{lf} and RR index. Open triangles and squares represent parent samples; filled triangles and squares represent pedogenic samples.

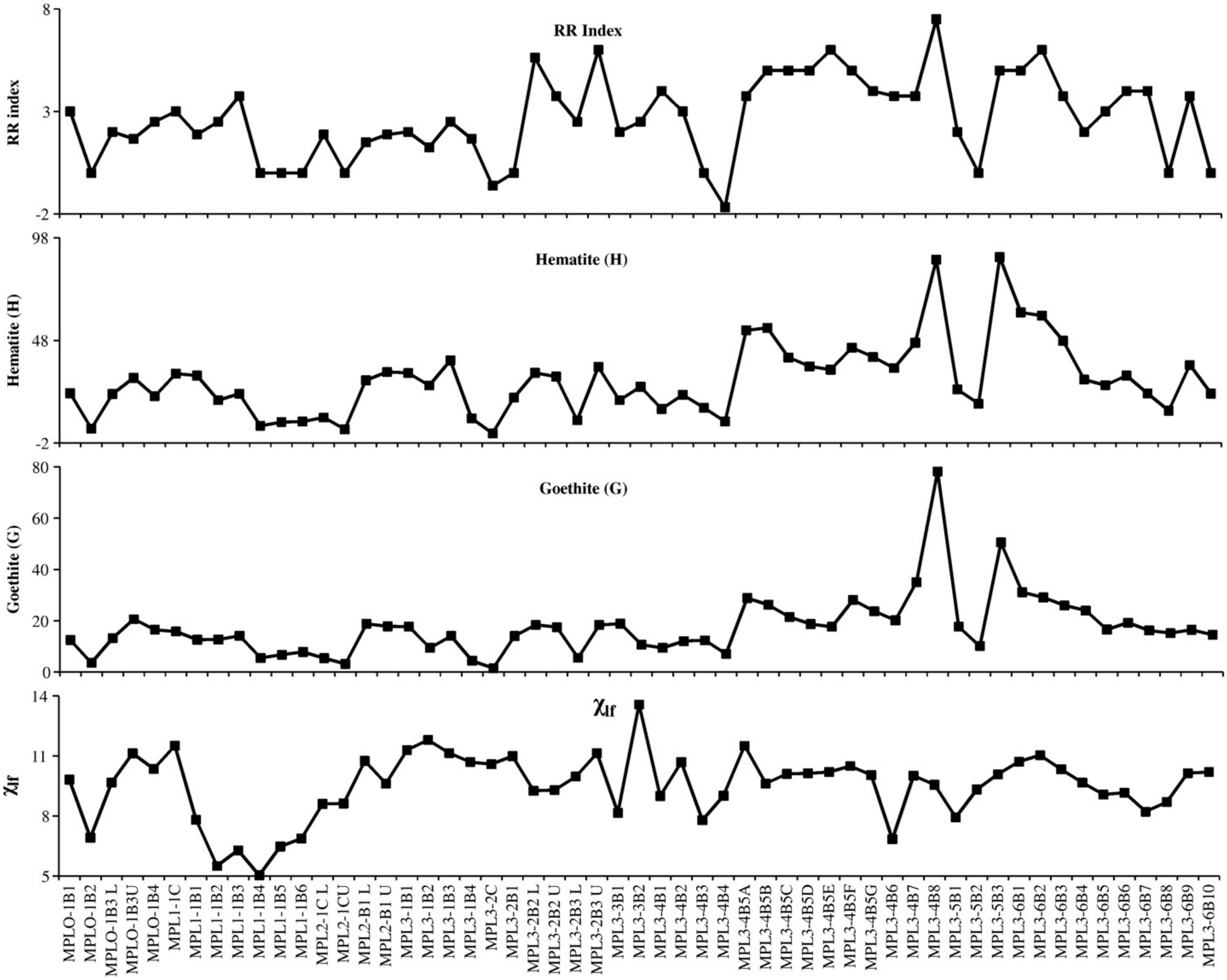

Fig. 10. Plots showing relation among RR index, hematite ($H \times 10^{-5}$ Am^2/kg), goethite ($G \times 10^{-5}$ Am^2/kg) and magnetic susceptibility ($\chi_{lf} \times 10^{-9}$ m^3/kg) of MR section paleosol samples.

5. Magnetic susceptibility comparison with redness rating

Similar to the elemental mobility, the soil color is predominantly controlled by the production and mobilization of the secondary iron oxides and hydroxides. The detailed comparison of χ_{lf} with RR index for each profile shows a consistent trend for majority of the horizons (Fig. 9). Higher RR index reflecting intensity of the red hue, the paleosols showing 5YR–7.5YR colors are anticipated to be hematite rich. Similarly, the lower RR index showing the predominant shift in the hue towards yellow (10YR–2.5Y–5Y) suggest significant presence of goethite.

In general, χ_{lf} for the hematite (H) is quite higher than goethite (G) whereas the saturation IRM for goethite is higher than hematite (Collinson, 1983; Thompson and Oldfield, 1986; Dunlop and Ozdemir, 1997). However, yet the distinction between hematite and goethite based on routine rock magnetic properties is difficult due to overlapping nature of susceptibility and IRM spectra for these minerals. Sangode and Bloemendal (2004) and Kumaravel et al. (2005b) suggested the parameters G (~IRM acquired between higher fields i.e., >1 T) and H (IRM acquired between ~0.5 and 1 T) for the Siwalik paleosols. We produce the curves for RR index, H, G and magnetic susceptibility in Fig. 10. The plots show that the RR index is controlled by a combination of goethite and hematite, and also by the magnetic susceptibility except at few horizons where magnetite is added to the mixture (Fig. 10). This indicates that when the magnetic susceptibility shows significant correlation with RR index it is predominantly controlled by hematite, the good correlation shows a combination of goethite and hematite and the poor correlation indicates a mixture of magnetite–maghemite, hematite and goethite. As the susceptibility for ferrimagnetic mineral (magnetite) is significantly higher than goethite and hematite, even minor amounts of magnetite formed by pedogenic process can greatly alter the χ_{lf}.

These first order relations may be useful for large scale mapping and correlation of the paleosols as in the Himalayan foreland basin. However more detailed studies such as CBD and Diffuse Reflectance Spectra (e.g., Balsam et al., 2004; Torrent et al., 2006) are warranted to resolve a quantitative relation amongst magnetic susceptibility, elemental mobility and the Munsell color indices.

6. Conclusions

Sympathetic variation of magnetic susceptibility with mobile and immobile elements due to pedogenesis is discernible from the present study on the Siwalik paleosols of the Himalayan Foreland Basin indicating a strong control of magnetic susceptibility over pedogenic processes. Further the co-variation amongst the Munsell color parameter of redness rating, magnetic susceptibility and the goethite–hematite content is observed. The color and susceptibility relation fails where the mineralogy becomes of mixed nature (magnetite + hematite + goethite). Several empirical relations can therefore be drawn from the susceptibility, soil color and geochemical indices within the Siwalik paleosol sequence for its widespread application elsewhere.

Acknowledgements

The Director, Wadia Institute of Himalayan Geology, Dehra Dun is thankfully acknowledged for providing necessary facilities. We thank anonymous referees for their critical and constructive reviews that have helped much in revising and improving the manuscript. Mr. Rakesh Kumar in the Palaeomagnetic lab WIHG is acknowledged for assisting during laboratory analysis. VK is thankful to the Director, Indian Institute of Geomagnetism, Navi Mumbai for encouragement and SJS is thankful to the Head, Department of Geology, University of Pune, for necessary help. This work was carried out under the research grant ESS/23/VES/146/2001 funded by Ministry of Science and Technology, New Delhi, India.

References

Balsam, W., Ji, J.F., Chen, J., 2004. Climatic interpretation of the Luochuan and Lingtai loess sections, China, based on changing iron oxide mineralogy and magnetic susceptibility. Earth Planet. Sci. Lett. 223, 335–348.
Barrón, V., Torrent, J., 1987. Origin of red-yellow mottling in a Ferric Acrisol of southern Spain. Z. Pflanzenernähr. Bodenkd. 150, 308–313.
Blavet, D., Mathe, E., Leprun, J.C., 2000. Relation between soil colour and waterlogging duration in a representative hillside of the West African granite–gneissic bedrock. Catena 39, 187–210.
Collinson, D.W., 1983. Methods in rock magnetism and palaeomagnetism: techniques and instrumentation. Chapman and Hall Publication. 503p.
de Jong, E., Pennock, D.J., Nestor, P.A., 2000. Magnetic susceptibility of soils in different slope positions in Saskatchewan, Canada. Catena 40, 291–305.
Dunlop, D.J., Ozdemir, O., 1997. Rock Magnetism: Fundamentals and Frontiers. University press, Cambridge. 488p.
Evans, M.E., Heller, F., 2001. Magnetism of loess/paleosol sequences: recent developments. Earth-Sci. Rev. 54, 129–144.
Evans, M.E., Heller, F., 2003. Environmental magnetism: Principles and applications of enviromagnetics. International Geophysics Series, Academic press. pp 293.
Fine, P., Singer, M.J., La Ven, R., Verosub, K.L., Southard, R.J., 1989. Role of pedogenesis in distribution of magnetic susceptibility in two California chronosequences. Geoderma 44, 287–306.
Fine, P., Singer, M.J., Verosub, K.L., TenPas, J., 1993. New evidence for the origin of ferrimagnetic minerals in loess from China. Soil Sci. Soc. Am. J. 57, 1537–1542.
Fitzpatrick, E.A., 1986. Soils, their formation, classification and distribution. ELBS, Longman, Hong Kong. 353 p.
Grimley, D.A., Arruda, N.K., 2007. Observations of magnetite dissolution in poorly drained soils. Soil Sci. 172, 968–982.
Grimley, D.A., Vepraskas, M.J., 2000. Magnetic susceptibility for use in delineating hydric soils. Soil Sci. Soc. Am. J. 64, 2174–2180.
Grimley, D.A., Arruda, N.K., Bramstedt, M.W., 2004. Using magnetic susceptibility to facilitate more rapid, reproducible, and precise delineation of hydric soils in the midwestern USA. Catena 58, 183–213.
Hanesch, M., Scholger, R., 2005. The influence of soil type on the magnetic susceptibility measured throughout soil profiles. Geophys. J. Int. 161, 50–56.
Heller, F., Liu, T.S., 1984. Magnetism of Chinese loess deposits. Geophys. J. Roy. Astron. Soc. 77, 125–141.
Johnson, G.D., 1977. Paleopedology of Ramapithecus-bearing sediments, North India. Geol. Rundsch. 66, 192–216.
Kampf, N., Schwertmann, U., 1983. Goethite and hematite in a climosequence in southern Brazil and their application in classification of kaolinitic soils. Geoderma 29, 27–39.
Karunakaran, C., Rao, R., 1976. Status of exploration for hydrocarbons in the Himalayan region: contribution to stratigraphy and structure. Geol. Surv. India Misc. Publ. 41, 1–66.
Kukla, G., Heller, F., Liu, X.M., Xu, T.C., Liu, T.S., An, Z.S., 1988. Pleistocene climates in China dated by magnetic susceptibility. Geology 16, 811–814.
Kumar, R., 1993. Coalescence megafan: multistorey sandstone complex of the late-orogenic (Mio-Pliocene) sub-Himalayan belt, Dehra Dun, India. Sediment. Geol. 85, 327–337.
Kumar, R., Tandon, S.K., 1985. Sedimentology of Plio-pleistocene late orogenic deposits associated with intraplate subduction—the Upper Siwalik subgroup of a part of Panjab Sub-Himalaya, India. Sediment. Geol. 105, 1–59.
Kumar, R., Ghosh, S.K., Mazari, R.K., Sangode, S.J., 2003. Tectonic impact on the fluvial deposits of Pleistocene Himalayan Foreland Basin, India. Sed. Geol. 158, 209–234.
Kumar, R., Sangode, S.J., Ghosh, S.K., 2004. A multistorey sandstone complex in the Himalayan Foreland Basin, NW Himalaya, India. J. Asian Earth Sci. 23, 407–426.
Kumaravel, V., Sangode, S.J., Kumar, R., Siva Siddaiah, N., 2005a. Magnetic polarity stratigraphy of Plio-Pleistocene Pinjor formation (type locality), Siwalik group, NW Himalaya, India. Curr. Sci. 88 (9), 1453–1461.
Kumaravel, V., Sangode, S.J., Siva Siddaiah, N., Kumar, R., 2005b. Rock magnetic characterization of pedogenesis under high energy depositional conditions: a case study from the Mio-Pliocene Siwalik fluvial sequence near Dehra Dun, NW Himalaya, India. Sed. Geol. 177, 229–252.
Kumaravel, V., Sangode, S.J., Siva Siddaiah, N., Kumar, R., 2009. Major element geochemical variations in a Miocene–Pliocene Siwalik paleosol sequence: implication to soil forming processes in the Himalayan Foreland Basin. J. Geol. Soc. India 73, 759–772.
Liu, Q.S., Deng, C.L., Torrent, J., Zhu, R.X., 2007. Review of recent developments in mineral magnetism of the Chinese loess. Quat. Sci. Rev. 26, 368–385.
Maher, B.A., 1998. Magnetic properties of modern soils and Quaternary loess paleosols: paleoclimatic implications. Palaeogeogr. Palaeoclimatol. Palaeoecol. 137, 25–54.
Maher, B.A., Thompson, R., 1992. Paleoclimatic significance of the mineral magnetic record of the Chinese loess and paleosols. Quat. Res. 37, 155–170.
Mullins, C.E., 1977. Magnetic susceptibility of the soil and its significance in soil science: a review. J. Soil Sci. 28, 223–246.
Munsell color, 2000. Munsell soil color charts. Gretag Macberth, New York.
O'Reilly, W., 1984. Rock and Mineral Magnetism. Glasgow, Blackie. pp 220.
Plice, M.J., 1942. Factors affecting soil color (progress report-1). Proc. Okla. Acad. Sci. 23, 49–51.
Plice, M.J., 1945. Factors affecting soil color (progress report-2). Proc. Okla. Acad. Sc. 33–34.
Retallack, G.J., 1995. Paleosols of Siwalik group as a 15 Ma record of south Asian palaeoclimate. Mem. Geol. Surv. India 32, 36–51.
Sangode, S.J., Bloemendal, J., 2004. Pedogenic transformation of magnetic minerals in Pliocene–Pleistocene palaeosols of the Siwalik Group, NW Himalaya, India. Palaeogeogr. Palaeoclimatol. Palaeoecol. 212, 95–118.
Sangode, S.J., Kumar, R., Ghosh, S.K., 1996. Magnetic polarity of the Siwalik sequence of Haripur area (H.P), NW Himalaya. J. Geo. Soc. India 47, 683–704.
Sangode, S.J., Kumar, R., Ghosh, S.K., 1999. Paleomagnetic and rock magnetic perspectives on the post-collisional continental sediments of the Himalaya, India. In: Radhakrishna, T., Piper, J.D.A. (Eds.), The Indian Sub-Continent and Gondwana: A Paleomagnetic and Rock Magnetic Perspective: Memoir Geol. Soc. of India, vol. 44, pp. 221–248.
Sangode, S.J., Kumaravel, V., Bloemendal, J., Kumar, R., 2008. Effect of burial and compaction on soil magnetic properties: results from soil–paleosol sequences in the Himalayan Foreland, India. Palaeogeogr. Palaeoclimatol. Palaeoecol. 267, 235–244.
Scheinost, A.C., Schwertmann, U., 1999. Color identification of iron oxides and hydroxysulfates: use and limitations. Soil Sci. Soc. Am. J. 63, 1463–1471.
Schwertmann, U., 1993. Relations between iron oxides, soil color, and soil formation. Soil Color: Soil Sci.Soc. Am. Spec. Publ., vol. 31, pp. 51–69. Madison.
Singer, M.J., Verosub, K.L., Fine, P., TenPas, J., 1996. A conceptual model for the enhancement of magnetic susceptibility in soils. Quat. Int. 34–36, 243–248.
Siddaiah, N.S., Sangode, S.J., 2005. Paleosol development in the Siwalik Foreland Basin: a linkage with uplift, sedimentation and basin subsidence. Himal. Geol. 26 (2), 367–380.
Stacey, F.D., Banerjee, S.K., 1974. The physical principles of rock magnetism. Elsevier, Amsterdam. pp 195.
Thakur, V.C., 1998. Structure of the Chamba nappe and position of the Main Central Thrust in Kashmir Himalaya. J. Asian Earth Sci. 16, 269–282.
Thompson, R., Oldfield, F., 1986. Environmental magnetism. Allen and Unwin press, London.
Thomas, J.V., Parkash, B., Mohindra, R., 2002. Lithofacies and paleosol analysis of the Middle and Upper Siwalik Group (Plio-Pleistocene), Haripur–Kolar section, Himachal Pradesh, India. Sed. Geol. 150, 343–366.
Torrent, J., Barrón, V., 1993. Laboratory measurement of soil color: theory and practice. In: Bigham, J.M., Ciolkosz (Eds.), Soil Color. Soil Science Society of America, pp. 21–33.
Torrent, J., Barrón, V., 2003. Iron oxides in relation to the colour of mediterranean soils. Applied Study of Cultural Heritage and Clays. Consejo Superior de Investigaciones Científicas, Madrid, pp. 377–386.
Torrent, J., Schwertmann, U., 1987. Influence of hematite on the colour of red beds. J. Sed. Petrol. 57, 682–686.
Torrent, J., Schwertmann, U., Schulze, D.G., 1980. Iron oxide mineralogy of some soils of two river terrace sequences in Spain. Geoderma 23, 191–208.
Torrent, J., Schwertmann, V., Fechter, H., Alférez, F., 1983. Quantitative relationships between soil color and hematite content. Soil Sci. 136, 354–358.
Torrent, J., Barrón, V., Liu, Q.S., 2006. Magnetic enhancement is linked to and precedes hematite formation in aerobic soil. Geophys. Res. Lett. 33, L02401. doi:10.1029/2005GL024818.
Valdiya, K.S., 1998. Dynamic Himalaya. University Press, Hyderabad, India. pp 178.
Verosub, K.L., Fine, P., Singer, M.J., TenPas, J., 1993. Pedogenesis and paleoclimate: interpretation of the magnetic susceptibility record of Chinese loess/paleosol sequences. Geology 21, 1011–1014.
Williams, M., 1992. Evidence for the dissolution of magnetite in recent Scottish peats. Quat. Res. 37, 171–182.
Williams, R.D., Cooper, J.R., 1990. Locating soil boundaries using magnetic susceptibility. Soil Sci. 150, 889–895.
Willis, B.J., Behrensmeyer, A.K., 1995. Fluvial systems in the Siwalik Miocene and Wyoming paleogene. Palaeogeogr. Palaeoclimatol. Palaeoecol. 115, 13–35.
Zaleha, M.J., 1997. Siwalik paleosols (Miocene, northern Pakistan): genesis and controls on their formation. J. Sediment. Res. 67 (5), 821–839.